Jordan Journal of Civil Engineering, Volume **14**, No. **1**, **2020**

The Behavior of Concrete-Filled Plastic Tube Specimens under Axial Load

Nwzad Abduljabar Abdulla

Assistant Professor, Department of Civil Engineering, Salahaddin Univ., Kirkuk Rd., Erbil, Iraq.
E-Mail:anwzad@yahoo.com

ABSTRACT

Plastic uPVC tubes were used to encase concrete subjected to compression load. Two series of specimens were tested to evaluate the contribution of plastic tube (PT) to enhancing strength and improving ductility of concrete in slender specimens subjected to axial load. The first series included nine concrete-filled plastic tube (CFPT) columns with diameter-to-thickness ratio (*D/t*) varying from 13.8 to 22. For comparison, series two contained four concrete-only specimens with variable slenderness ratio (*KL/r*). At the top end, the columns were tested for rotation free and translation fixed end conditions. The main parameters of the study included *the D/t* ratio, the rotations of the loading platen and the length-to-diameter ratio (*L/D*). Deformed shape, failure mode, ultimate strength, lateral deformation, angular rotation at column end, ductility and toughness were studied. With increased slenderness, the load-carrying capacity reduced and the composite column system underwent substantial compression softening past the peak load, depending on the end rotation. The use of polymeric tube resulted in progressive failure instead of sudden and explosive failure associated with plane concrete columns. The lateral displacement at failure increased from an average of 3.4 mm for normal columns to a maximum value of 95 mm for CFPT columns (1-6). A similar trend was observed for angular rotation and ductility of the composite system, which increased by 20 and 11 folds, respectively.

KEYWORDS: Plastic tube, Failure mode, Compression softening, Length effect, Tube influence, Ductility.

INTRODUCTION

Concrete cover plays a vital role in the protection of the concrete core and its reinforcing steel. Loss of cover due to erosion in a marine environment, excessive shrinkage micro-cracks, de-lamination, cracking and chipping under high compressive stresses could lead to considerable damage in the concrete cross-section. The ingress of impurities into the uncovered concrete might initiate steel corrosion as well as durability and serviceability losses. Furthermore, traditional column formworks, timber or steel, have many drawbacks and disadvantages which could be overcome using polyvinyl chloride (PVC) tubes. The concrete-filled plastic tube is a composite system in which the thin-walled plastic tube (PT) has several roles. As a formwork, it will prevent any moisture loss necessary for the setting and hydration of fresh concrete and protect concrete from thermal changes. By sealing the hardened concrete, it will eliminate the time-consuming and costly curing process. A good finished final member is achieved by closing the surface pores and making the column impermeable. The PT can confer a protective cover to concrete in substructures in contact with soil (pile) or marine environment (bridge columns and piers). Surface sealants applied on the tube surface would further improve the durability of the tubular system. One of the early studies on the structural

Received on 8/11/2019.
Accepted for Publication on 5/2/2020.

application of plastic polymer tube was the CFPT and acrylonitrile-butadiene-styrene (ABS) columns, conducted by Kurt (1978). The author reported that the structural behavior of PT was similar to the behavior of spiral reinforcement. Short CFPT specimens, tested under compression, yielded a toughness index ranging from 0.6 to 0.85, which is an important factor for safe design (Abdulla, 2020). The acceptable behavior of a structure is largely associated with the sufficient rotational capacity of the critical sections (Lopes and Bernardo, 2003). Rahai et al. (2009) performed tests on the cyclic performance of composed materials and suggested, depending on the circumstances, that an acceptable substitute for steel tubes is polymeric materials, such as fiber-reinforced polymer (FRP) sheets (Abdalla et al., 2019) and PVC tubes. FRP materials exhibit linear elastic stress-strain relationships with a failure strain ranging from 1.0% to 2.5% (Abdelkarim and El-Gawady, 2015), compared to 46% for the PT (Fakharifar and Chen, 2016). The objective of the current study is to explore the failure modes and identify key parameters influencing the mechanical behavior of such a composite system under axial compression load *via* a series of experimental tests with various *D/t* and *L/D* ratios. Such composite systems could offer an economical solution for the protection of piles and piers found in aggressive chloride environments.

TEST PROGRAM

Fabrication and Testing

The mix proportion of concrete was 1:2:4 with a w/c ratio of 0.5 and a maximum aggregate size of 20 mm. The concrete was mixed and placed in the laboratory using a 0.07m^3 capacity drum mixer. Two series of specimens were cast. Series one included nine CFPT columns, while series two had four normal concrete specimens (Fig.1). Besides, each series had several short specimens with *an L/D* ratio of two for comparison purposes. The mechanical properties of PT and mix details are summarized in Table 1. Previous research focused on columns with *L/D* ratios between 2 and 5. The size of some of the columns tested was equivalent to 1/3 of the full-scale column. A swiveling loading cell with a maximum loading capacity of 500kN was used to apply axial load and to ascertain the pin-ended restraint condition, which resulted in the unrestricted rotation of the upper end of the columns, while the lower ends were supported on a stiff flat base that rested on strong floor (Figure 2(a)). Four linear displacement transducers (LVDTs) and two inclinometers (supported on top of the swiveling loading platen) were used to measure the lateral displacement and monitor the rotation of the upper end of the column. Although a load control procedure was used to test both the normal and CFPT columns, it was not possible to trace the response of the normal specimens beyond the peak load. For end-fixtures, the ideal conditions approximated and the K value, effective length factor which was a function of the rotational restraint at the column ends, was taken as 0.8, while the *L/D* ratio for short specimens was approximated to 6.8 (0.8*L*/0.25*D*=22). The short specimens were tested in another machine with a testing capacity of 1000kN and having an articulated head (Figure 2(b)). Coupon testing is shown in Figure 2(c).

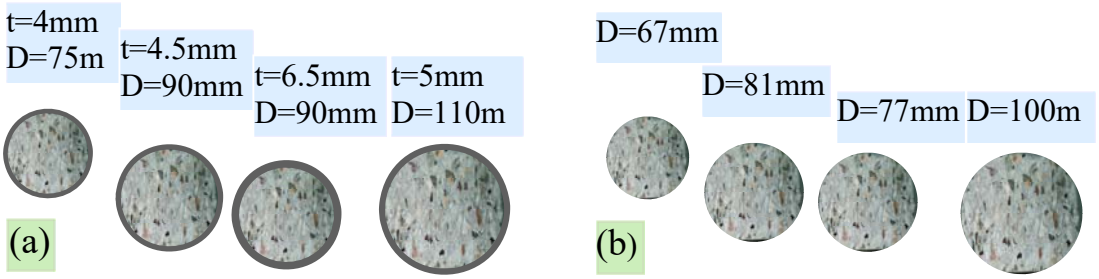

Figure (1): Cross-sections of (a) series 1 and (b) series 2 specimens

TEST RESULTS

Failure Modes

Short only PT specimens exhibited elephant's foot buckling failure mode (Fig. 3(a)). Typical failure modes of short PT and CFPT are shown in Figs.3(b) and 3(c), respectively. The coupons before and after test are shown in Fig. 4. For slender CFPT, deformations produced cracks in concrete, which increased with the increase of load; tensile cracks developed in the stretching side and concrete crushing in the shortening side of the tested specimen. Finally, yielding of the plastic tube was started, manifested itself in terms of a fine line with a color change from gray to whitish, followed by local buckling due to the loss of tangential surface contacts on the compression side and overall buckling (Fig.5 (a)). Local buckling phenomena became more pronounced in the slender CFPT specimens with small *D/t* ratios which underwent extensive plastification on the central part, 1-2, 1-3, 1-6, 1-7 and 1-9. With increased *D/t* ratio, the specimen became amply stiff and the critical section shifted more and more upward due to end rotations, leading to approximately 45^o shear failure surface in the inner core and the tube skin sustained considerable slippage of the concrete core (specimens 1-1 and 1-4 in Fig.5 (a)). The failure zone length (L_{PT}) of slender CFPT specimens, taken from the top of the specimen to the center of the critical failure section, was measured at yield load ($L_{PT.Y}$) and ultimate load ($L_{PT.U}$), respectively (Table 2). From Table 2 and Fig. 5(b), values of L_{PT} were not equal to the half-length of the column and depended on column eccentricity, vertical alignment, end conditions and rotations, failure pattern and the shape of buckling or curvature. All the concrete-only specimens failed in a brittle sudden explosive manner due to the lateral splitting of concrete at more than one location (Fig. 5(c)).

Table 1. Specimen dimensions and material properties

S.	*No.*	*L mm*	*D mm*	D_{EQ} *mm*	*t mm*	*D/t*	L/D_{EQ}	*KL/r*	*Material details*
1	1-1	1200	110	111.6	5.0	22.0	10.7	34.4	Concrete: Mix:1:2:4 W/C ratio=0.5 M.A.S=20mm f_{cu}=30MPa PVC tube: Density:1.32gr/cm^3 f_{yp}=40.53MPa f_{cp}=40.0MPa Elongation at break=38% E=4000MPa Impact test= 0.333J/cm Burst pressure= 3.3MPa Tube mass/unit length=1.27 kg/m
	1-2	1200	90	92.0	6.5	13.8	13.0	41.7	
	1-3	1200	90	91.4	4.5	20.0	13.1	42.0	
	1-4	1100	110	111.6	5.0	22.0	9.85	31.5	
	1-5	1000	110	111.6	5.0	22.0	8.96	28.7	
	1-6	1000	75	76.2	4.0	18.7	13.1	42.0	
	1-7	1000	90	91.4	4.5	20.0	10.94	35.0	
	1-8	900	110	111.6	5.0	22.0	8.06	25.8	
	1-9	750	75	76.2	4.0	18.7	9.84	31.5	
	1-10s	150	75	76.2	4.0	1.57	1.96	6.3	
	1-11s	180	90	91.4	4.5	1.97	1.97	6.3	
	1-12s	180	90	92.0	6.5	1.95	1.96	6.3	
	1-13s	220	110	111.6	5.0	1.97	1.97	6.3	
2	2-1	1100	67		-	-	16.4	52.5	
	2-2	1000	100		-	-	10.0	32.0	
	2-3	1100	100		-	-	11.0	35.2	
	2-4	1200	100		-	-	12.0	38.4	
	2-5	1200	81		-	-	15.0	48.0	
	2-6s	140	67		-	-	2.1	6.72	
	2-7s	160	81		-	-	1.97	6.30	
	2-8s	200	100		-	-	2.0	6.40	

(S. = series, No. = specimen number, L= length, D= diameter, t= thickness, -= not applicable).

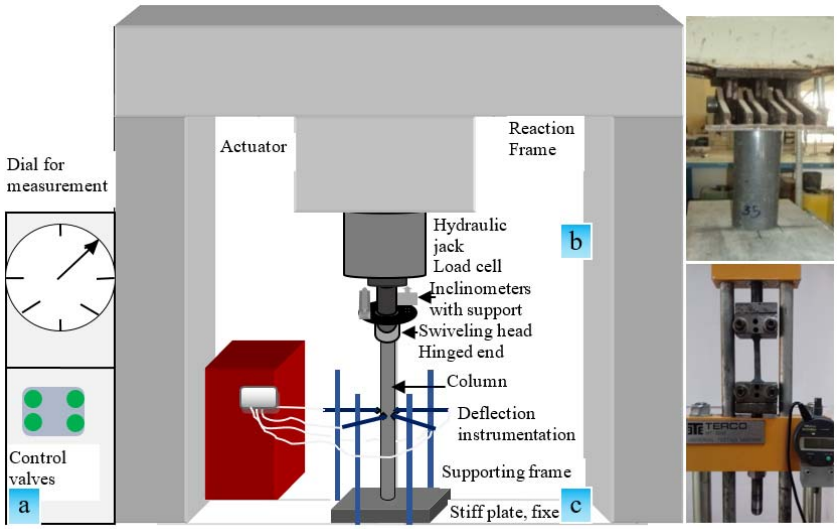

Figure (2): Test setup for (a) slender specimens, (b) stub columns and (c) coupons

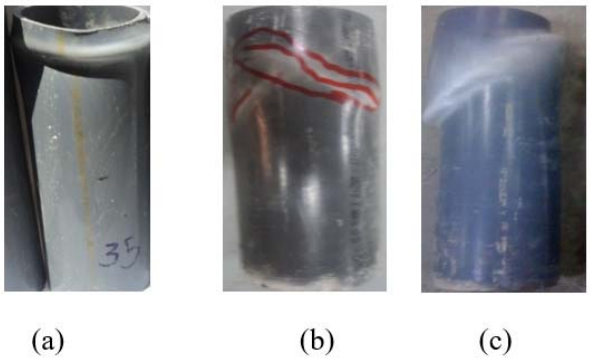

Figure (3): Tested specimens (a) plastic tube, (b) CFPT (elephant foot) and (c) CFPT (shear mode)

Figure (4): Coupon (a) before test and (b) after test

Load-Deflection Relationship

The test results for yield load (P_Y) and ultimate load (P_U) carried by each specimen and the corresponding rotations (θ_Y, θ_U) and lateral displacements (δ_Y, δ_U) are summarized in Table 2. The coupon stress-strain relationship is shown in Fig. 6. In the flexural failure mode (buckling), the CFPT specimens exhibited the largest lateral displacement near the mid-height, resulting in fissuring and crushing of concrete core in the compression side and tensile cracks in the other side. According to the classification of ACI 440.2R-08 for the stress-strain behavior of the RC column, the CFPT, based on the load-deformation curve, can be considered as lightly confined with compression softening. The load- deflection curves exhibited an initial elastic zone, yielding and post-peak zones (Fig. 7). The lateral displacement increased from an average of 3.4 mm (for normal columns) to a maximum value of 95 mm for CFPT (1-6), leading to a single permanent curvature at the ultimate load. In contrast to CFPT, plain concrete columns had an abrupt descending branch (Fig. 8).

Load-Rotation Relationship

The rotational response of CFPT specimens with load was similar. At the initial stage, the ascending part was elastic linear. The second part of the curve, yield to

peak, had forms that varied from column to column, depending on several factors, including *KL/r* ratio, tube diameter and thickness. Past peak load, the specimens with large *D/t* ratio showed steeper falling branch in contrast to specimens with smaller *D/t* ratio which exhibited more uniform descending branches and increase in the rotation capacity (1-6, 1-7 and 1-3) (Fig. 9). The concrete only columns (specimens 2-1, 2-2, 2-3 and 2-4) showed no increase in the rotational capacity at and beyond peak loads, which was a clear sign of brittleness.

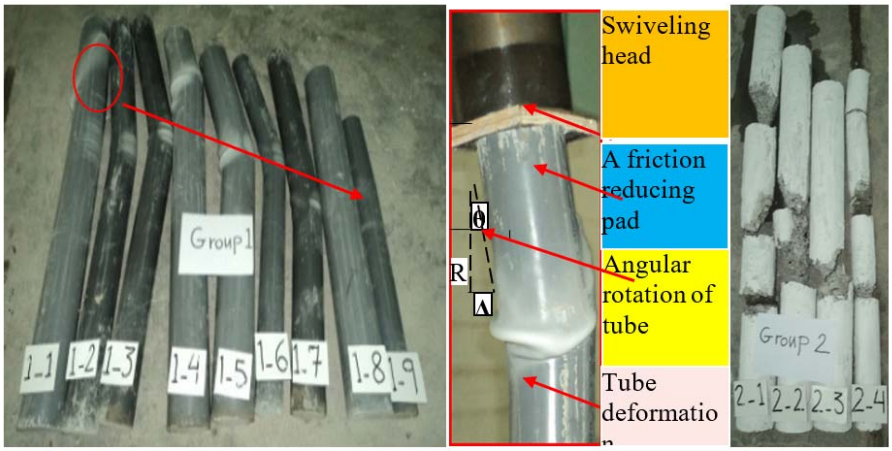

Figure (5): Slender specimens (a) series 1, (b) specimen (1-4) (during testing) and (c) series 2

Table 2. Test results for series one and series two specimens

No.	δ_y *mm*	θ_{ey} *rad10^{-2}*	*Py MPa*	L_{PTy} *mm*	δ_u *mm*	θ_u *rad10^{-2}*	P_U MPa	L_{PTu} mm	$\theta_{y.eff}$ *rad10^{-2}*	μ
1-1	3.33	3.07	200.0	150	10.0	6.5	150	160	2.9	1.41
1-2	2.59	2.67	120.0	480	75.0	13	40	480	2.4	1.15
1-3	2.23	1.99	110.0	460	90.1	17	30	460	1.85	4.24
1-4	3.50	3.37	219.0	390	35.0	7.5	90	402	3.25	1.26
1-5	3.29	3.10	197.0	343	50.7	17.8	70	348	3.08	1.48
1-6	2.20	1.47	80.00	360	95.0	24.4	28	360	1.4	3.34
1-7	2.40	2.50	135.0	435	85.0	16	27	439	2.39	2.13
1-8	4.40	4.00	283.0	-	-	-	-	-	-	-
1-9	3.00	1.69	104.0	358	14.1	3.2	80	358	1.55	1.83
1-10s	3.5	-	164	60	-	-	-	-	-	-
1-11s	3.9	-	217	57	-	-	-	-	-	-
1-12s	3.8	-	244	53	-	-	-	-	-	-
1-13s	4.4	-	326	45	-	-	-	-	-	-
2-1	1.35	1.45	57	-	1.35	1.45	57	-	1	1
2-2	3.31	3.6	155	-	3.31	3.6	155	-	1	1
2-3	3.52	2.6	154.5	-	3.52	2.6	154.5	-	1	1
2-4	3.35	2.25	135	-	3.35	2.25	135	-	1	1
2-5	-	-	-	-	-	-	-	-	-	-
2-6s	-	-	106.2	-	-	-	-	-	1	-
2-7s	-	-	155.2	-	-	-	-	-	1	-
2-8s	-	-	236.5	-	-	-	-	-	1	-

(L_{PTy} is the failure zone length, the vertical distance measured from top of specimen to the centre of critical section at yield load. L_{PTu} is the failure zone length, the distance measured from top of specimen to the centre of critical section at ultimate (failure) load. P_U=failure load, *KL/r*= slenderness ratio. *r*=radius of gyration. *s*=short column (L/D=2). δ_y= measured lateral displacement at tube yield at mid-height of column. δ_u = ultimate lateral displacement. θ_y=angular rotation (in radians) at tube yield. θ_u=measured ultimate rotation (in radians). μ (ductility index) = δ_u/δ_y. I_θ (rotation index to characterize plastic rotation capacity) =θ_u/θ_y. 2/0.9: 2 is *L/D* ratio and 0.9 is diameter. - means not applicable or no data).

Deflection-Rotation Relationship

Fig. 10 displays the experimental rotation-deflection (θ-δ) relationship for CFPT tested columns. For CFPT, there was the elastic stage (a straight line with uniform slope) and the yield stage (red dashed line in Fig.10), followed by plastic stage (a sharp change in the slope) due to the formation of a plastic hinge, white patches, where the physical plastic rotation is higher and the curvature in the section is higher. Such behavior was a sign of considerable ductility due to the presence of the tube. Generally, the angular rotation increased the lateral deformation (buckling instability). No such observations were possible for series two specimens.

Physical Plastic Hinge Length (L_{PT})

Almost in all the CFPT specimens, the critical section was located in the upper half of the column and the corresponding eccentricity ($\delta_{C.S}$) was calculated from geometry. As shown in Fig.5(b), a large and non-linear curvature occurred in the physical plastic hinge zone with the length of L_{PT} and the magnitude of this curvature influencing the failure of the specimen (Gu et al., 2012). A stage was reached where the location separating the plastic from elastic parts was fundamentally fixed and was used to determine the physical plastic hinge length L_{PT}. At this location, the PT deformed considerably due to concrete core cracking, which yielded a considerable curvature at the cracked section. The values of L_{PT} of all the tested CFPT specimens were approximated in a logical manner and listed in Table 2. The physical plastic deformation zone is closely related to the equivalent plastic hinge length, which is a theoretical length that accounts for the plastic rotational capacity of the column (Paulay and Priestley, 1992).

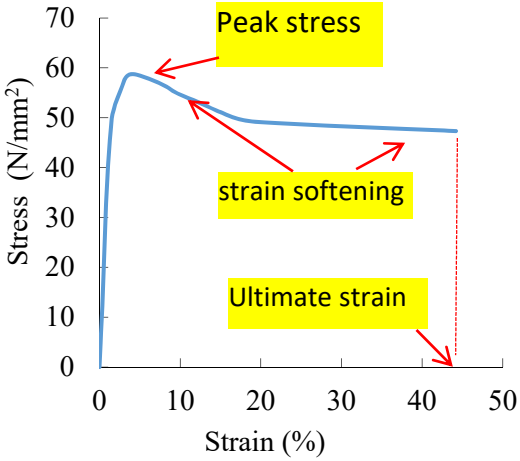

Figure (6): Stress-strain curve of coupon

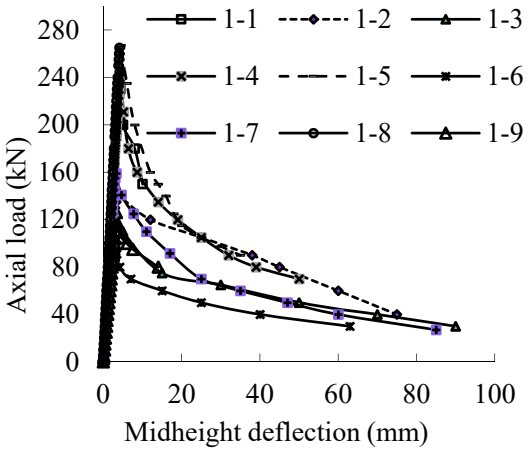

Figure (7): Load-deflection for series 1

MAIN PARAMETERS

Loading Platen Rotations

For slender CFPT specimens, the locations of the critical section and the softening of the descending branch of the load-deflection curve were influenced by the allowable rotation at the top end of the specimens. In specimens with a large *D/t* ratio, the critical section shifted upward under the influence of rotating platen. The measured experimental rotations are tabulated in Table 2. The ultimate rotations are also approximated as follows (Fig.5 (b)):

$$\theta_{U.cal}=\arctan\frac{\Delta}{R}; \quad (1)$$

where Δ is the deflection at the critical section, which

was approximated from simple geometry and R=physical plastic hinge length. The calculated values of rotation, Table 3, show good agreement with the measured values. The low-modulus tube provided low but uniform confining pressure against the lateral expansion of the concrete, resulting in compression-softening past peak load. However, the slenderness effect reduces confinement effectiveness and columns strengthened with transverse CFRP jacketing exhibited a response similar to slender non-strengthened RC columns (Tao and Yu, 2008).

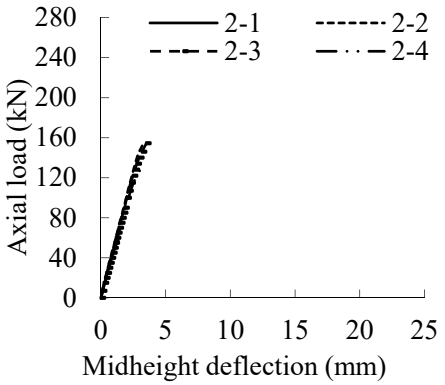

Figure (8): Load- deflection for series 2

Table 3. Test results compared with predicted results

No.	$\delta_{c.s}$ *mm*	$\theta_{U.cal}$ *rad10^{-2}*	$\theta_U/\theta_{U.cal}$	*f'cu* MPa	P_L *kN*	P_L/P_S Exp.	P_L/P_S Eq.5	P_L/P_S Eq.10	P_L/P_S Eq.13	P_L/P_S Eq.19
1-1	17.68	8.6	0.76	24.20	230	0.71	0.67	0.83	0.62	0.72
1-2	90	14.7	0.88	22.63	140	0.59	0.48	0.79	0.84	0.67
1-3	111	18.95	0.9	19.64	125	0.58	0.45	0.79	0.60	0.66
1-4	44.4	8.68	0.86	25.77	267	0.75	0.73	0.84	0.67	0.74
1-5	65.2	18.73	0.95	28.10	245	0.82	0.80	0.86	0.71	0.77
1-6	121.6	26.5	0.92	20.60	91	0.56	0.46	0.79	0.55	0.66
1-7	95.4	17.07	0.94	25.00	159	0.73	0.66	0.83	0.70	0.72
1-8	-	-	-	31.00	283	0.90	0.87	0.87	0.76	0.79
1-9	15.47	3.5	0.91	26.40	116.5	0.71	0.73	0.84	0.67	0.74
1-10s	-	-	-	37.10	-	-	-	-	-	-
1-11s	-	-	-	34.10	-	-	-	-	-	-
1-12s	-	-	-	38.40	-	-	-	-	-	-
1-13s	-	-	-	34.30	-	-	-	-	-	-
2-1	-	-	-	15.20	57	-	-	-	-	-
2-2	-	-	-	18.90	155	-	-	-	-	-
2-3	-	-	-	18.70	154.5	-	-	-	-	-
2-4	-	-	-	16.50	135	-	-	-	-	-
2-5	-	-	-	-	-	-	-	-	-	
2-6s	-	-	-	30.30	-	-	-	-	-	-
2-7s	-	-	-	30.20	-	-	-	-	-	-
2-8s	-	-	-	30.00	-	-	-	-	-	-
AAE%	-	-	-	-	-	-	9.4	25	12.4	7.8

(*f'cu*=compressive strength of composite or normal specimen. *s*=short column (L/D=2). P_L/P_S=ratio of peak load of long to short column. $\delta_{c.s}$ = calculated ultimate lateral displacement at the critical section (approximated from load-deflection curves using geometry). θ_c= calculated ultimate rotation measured in radians= arctan ($\delta_{c.s}$ /L_{PTu}). θ_u/θ_c = *ratio of* measured to calucated ultimate rotation).

Tube Thickness

The influence of the tube thickness was larger on short specimens and when the tube thickness was increased by 44%, from 4.5 mm for specimen (1-11s) to 6.5 mm for specimen (1-12s), there was a 13% increase in strength (Tables 1 and 3). However, for slender specimens, there was a very small increase in P_L/P_S ratio amounting to only 1% for the same diameter (0.9 m) and length (1.2 m). With the increase in tube thickness, the slope of the descending branch of the load-deflection curve declined more and the capacity to undergo rotation decreased.

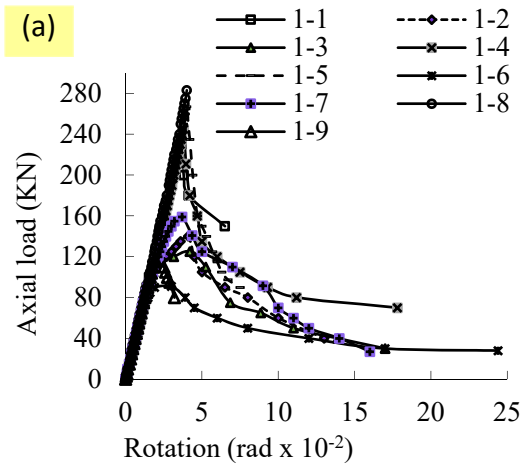

Figure (9): Load-rotation relationship for CFT

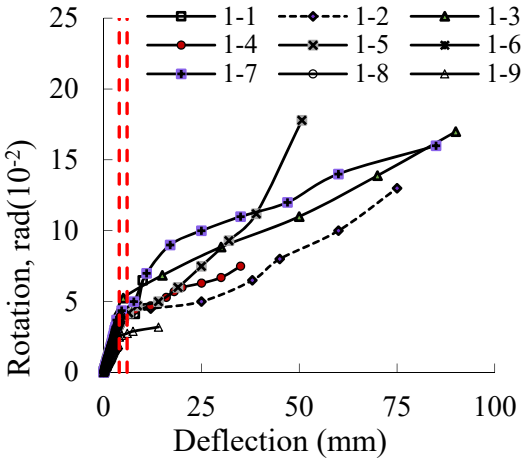

Figure (10): Rotation-deflection for CFPT

Effect of D/t Ratio

Local buckling phenomena were more pronounced in specimens with a small *D/t* ratio, where failure was close to the central part of the tube. Specimens with larger *D/t* ratios failed in the upper part of the tubes with extensive plastification. The *D/t* ratio of the tested CFPT ranged from 1.57 to 1.97 and from 13.8 to 22 for short and slender specimens, respectively (Table 1 and Fig.11). For *D/t* ratio of 22, the CFPT heights were 1.2, 1.1, 1.0 and 0.9 m, with corresponding KL/r ratios of 25, 30 and 35, respectively. There was an 11% reduction in strength when *the D/t* ratio was increased from 1.57 to 1.97 for short CFPT (Table 3). A similar trend was observed in slender CFPT specimens with (D=0.9 m and 1.2 m) when *the D/t* ratio was increased from 13.8 (1-2) to 20 (1-3) (Fig. 12).

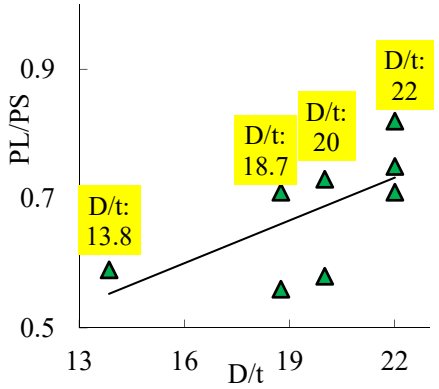

Figure (11): Effect of D/t ratio on P_L/P_S

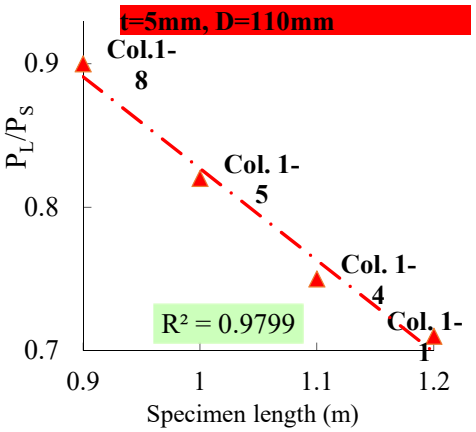

Figure (12): Variation of P_L/P_S with L

Tube Diameter

The increase in tube diameter yielded a considerable increase in P_L/P_S ratio. Such increase was mainly due to the increase in the resisting concrete area. The radial stiffness (K_R) of the confining plastic tube for different diameters of series one specimens was evaluated using thick wall cylinder theory (Timoshenko, 1970) utilizing:

$$K_R=\frac{2E}{(1+\upsilon)}\left[\frac{{D_{ex}}^2-{D_{in}}^2}{(D_{in})\left\{(1-2\upsilon).{D_{in}}^2-{D_{ex}}^2\right\}}\right] \quad (2)$$

where E= Young's modulus; υ = Poisson's ratio; D_{in} and D_{ex} = inner and outer diameters of the plastic tube, respectively. The computed values of K_R were plotted against D/t ratios, (Fig.13), showing a linear variation. As D/t ratio increased, K_R decreased. This behavour is ascribed to the increase in the area of the low modulus plastic tube. As D/t ratio was changed from 18.75 to 13.84, 20 and 22, the area of the plastic tube was increased by 91, 35 and 85%, respectively.

L/D Ratio

The CFPT specimens (1-7) and (1-2, 1-3, 1-6) with large L/D ratios experienced a large curvature around the midheight cross-section, due to direct and bending stresses. The effect of specimen length L on the P_L/P_S ratio for the same thickness (5 mm) and diameter (110 mm) was given in Fig. 12, where 20% increment in length (from 1 to 1.2 m) resulted in approximately a 14% reduction in P_L/P_S ratio. A similar trend was observed for specimens with thicknesses of 4.5 mm and 4 mm.

KL/r Ratio

The ultimate load capacity was reduced in combination with change in the lateral displacement as the slenderness ratio was increased (Table 2). However, this effect was not noticeable for series two columns and Fig.14 ascertains the influence of KL/r ratio on the ultimate load capacity of columns. Simple linear regression for each series yielded a straight-line trend. The effect of KL/r on series one columns (R^2=0.95) was more pronounced than in series two columns, despite the more scatter in the results of series two culumns (R^2=0.87) (Fig. 15). This behaviour is ascribed to the low stiffness of PT which makes the CFPT column more susceptible to instability. The limit for short column (L/D) was 6.8 and when it was increased to 13.3 (1-6), the strength was decreased by 44% of the equivalent short column. As the *KL/r* ratio increased, the $L_{PT.U}$ increased too, despite the weak correlation. The strength increased with an increase in *D/t* ratio. There was no clear trend for the variation of $L_{PT.U}$ with *D/t*, but generally, as *D/t* ratio increased (area of PT increased) $L_{PT.U}$ decreased. The low-modulus PT offered little confinement, but it was more effective in the longitudinal direction, where it resisted axial and bending stresses (Choi, 2019).

Gu et al. (2012) studied FRP-confined circular concrete columns and concluded that confinement increased the equivalent plastic hinge length when it was small, but reduced it when it was large. The results for the failure zone length (Fig. 13 (b)) were in line with the observations made by Gu et al. (2012) and a similar trend was observed by Wu and Jiang (2014), where an increase in confinement level (*D/t* in case of CFPT) reduced the equivalent plastic hinge length ($L_{PT.U}$ in case of CFPT). The θ_U-δ_U relationship for series one specimens was plotted in Fig.13c.

Ductility

Ductility was directly related to the rotation capacity and the δ-θ relationship was substantially dependent on the failure mode. The results of rotations for specimen 1-7 was idealized into an elastic-plastic graph and was used in combination with experimental load-rotation curve to calculate the rotation ductility index from:

$$\mu=\frac{\theta_U}{\theta_{y.eff}} \quad (3)$$

where θ_u was the maximum column rotation at the critical section corresponding to 20% degradation of peak load and $\theta_{y.eff}$ was the effective elastic rotation in the critical section at yield, determined from Fig.14. To

compare ductility levels reached by the tested specimens, the ductility rotation index was assessed and used for characterizing the ductile behavior of the tested columns. For slender CFPT (Fig. 7 (b)), ductility was slightly affected by the change in tube thickness and the thickness of PT had little influence on the initial stiffness and ultimate capacity. Although the plastic tube has increased the ductility of concrete columns several folds (Fig. 15), no direct comparison between CFPT and normal concrete columns was possible, since the response of the normal specimens beyond the peak load was very brittle and not traceable, despite using the same load control procedure for both normal and CFPT columns.

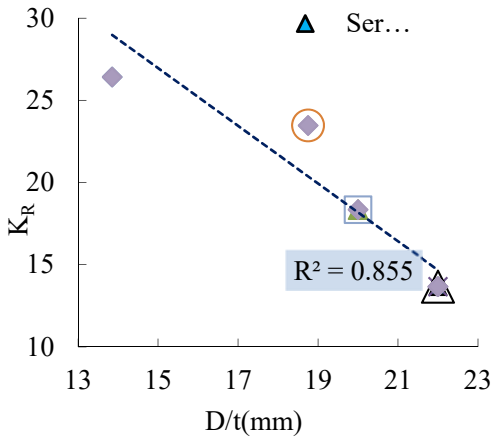

Figure (13): Effect of D/t ratio on K_R

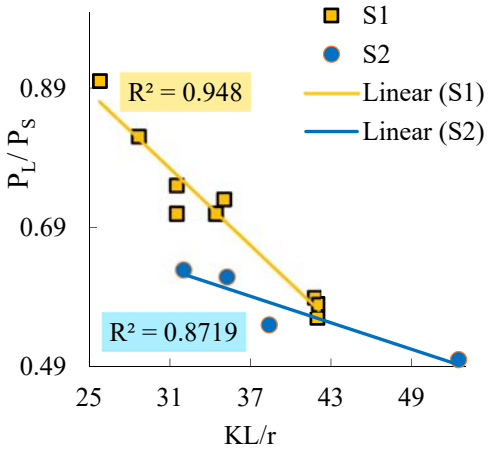

Figure (14): P_L/P_S *versus* KL/r

Table 4. Models for strength of slender CFPT columns

Source	Model	Symbol
Kwak and Kim (2004)	$P_L=1-\left\{(1-F)\left(\frac{e}{e_{min}}\right)^{\frac{1}{4}}\right\}P_S$ (4) $F=a+b\left(\frac{KL}{r}\frac{1}{100}\right)$ (5) $a=-0.15+1.12\rho_{PT}-6.23\rho_{PT}^2$ (6) $b=0.918+10.92\rho_{PT}+69.25\rho_{PT}^2$ (7) $\left(\frac{e}{e_{min}}\right)^{\frac{1}{4}}=1$ (8)	F= strength reduction coefficient; e=load eccentricity;e_{min}=minimum eccentricity; $\rho_{PT}=A_P/A_C$; A_P=area of plastic tube; A_C=area of concrete core.
Yang et al. (2015)	$P_L=(1-F)P_S$ (9) $F=1-0.005\lambda$ (10) $\lambda=\frac{KL}{r}$ (11)	λ =slenderness ratio.
Present study	$P_L=(1-F)P_S$ (12) $F=\left\{1.76-0.9n\left(\frac{L}{D_{EQ}}\right)+0.023n\left(\frac{L}{D_{EQ}}\right)^2\right\}$ (13) $n=\frac{E_{PT}}{E_C}$ (14) $r=D_{EQ}/4$ (15) $D_{EQ}=D+2t\frac{E_f}{E_C}$ (16) $Ec=4700\sqrt{f_c}$ (17)	n= modular ratio; $E_P$and E_C=modulus of elasticity of PT and concrete; D_{Eq}=equivalent diameter of composite system; L= length of specimen.
Present study	$P_L=(1-F)P_S$ (18) $F=1-0.008\left(\frac{KL}{r}+\frac{2t}{D_{EQ}}\right)$ (19)	t= tube thickness.

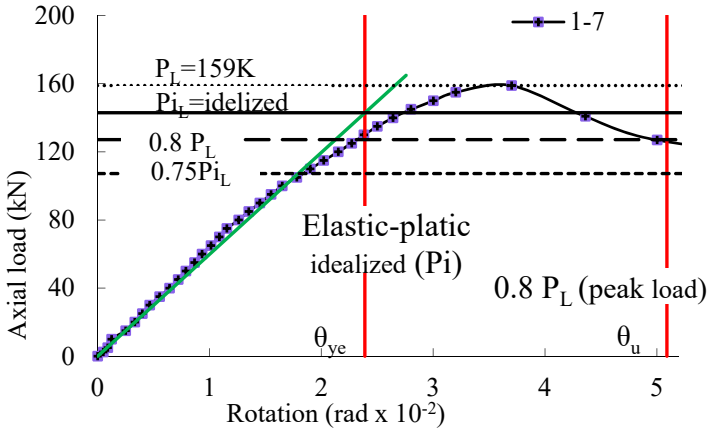

Figure (15): Ductility index calculations for specimen 1-7

Ultimate Strength

All the slender specimens had a KL/r ratio greater than 22 (ACI slenderness limit for unbraced columns). The P_L/P_S ratio increased with the increase in specimen cross-section. The plastic tubes provided the specimen with low confinement in the lateral direction, but additional strength in the longitudinal direction. For the same KL/r ratio, the ultimate strength of CFPT specimens was increased considerably compared with concrete-only specimens.

ANALYTICAL MODEL

Equation (4) proposed by Kwak and Kim (2004) and Equation (10) proposed by Yang et al. (2015) with buckling reduction factor (F) were adopted to predict the capacity of slender CFPT specimens (P_L) from their equivalent short columns (P_S) (Table 4). Based on the results of regression analysis of the experimental test data, two equations, (12) and (18), were developed (Table 4).

The developed Equation (18) yielded a better agreement between the predicted and experimental results. The accuracy of the four equations was checked using average absolute error (AAE) (Table 4). Equations (4) and (18) with AAE values of 9.4 and 7.8 might be used for the initial design of slender CFPT specimens until proper procedures and standard design methods are developed.

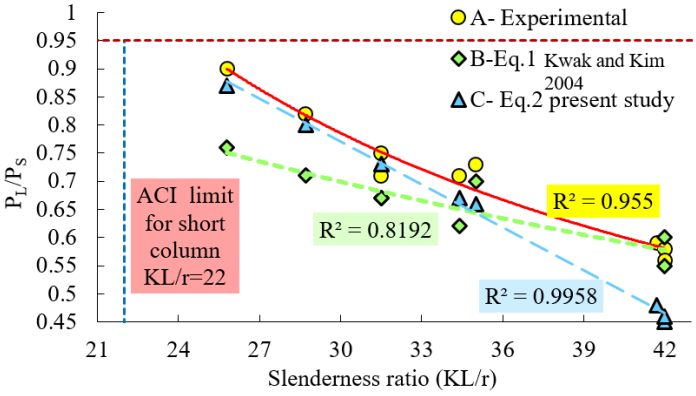

Figure (16): P_L/P_S *versus* slenderness ratio for experimental, Eq. 1 (Kwak and Kim, 2004) and proposed equation

CONCLUSIONS

Based on the results of this experimental investigation, the following conclusions were drawn:

(1) The capacity of CFPT to undergo rotation decreased generally with an increase in D/t ratio. The failure mode of all slender CFPT specimens is largely influenced by the swiveling loading platen (rotation of column upper end). Typical failure (buckling or shear) was marked by yielding of the tube at points of maximum stress concentration (compression and tension).

(2) Unlike normal columns, the CFPT specimens showed significant energy absorption capacity and continued to deform after the peak load was reached, resulting in compression softening with a gradual descending branch, which increased the area under the load-deflection curve.

(3) The lateral displacement at failure increased from an average of 3.4 mm for normal columns to a maximum value of 95 mm for CFPT (1-6). A similar trend was observed for angular rotation and ductility of the composite system, which increased by 20 and 11 folds.

(4) Slender CFPT specimens were more sensitive to length effect than concrete-only specimens. For the same D/t ratio, as the *KL/r* ratio was increased from 28.7 to 34.4, the ultimate strength was reduced from about 82% of the equivalent short column, P_L/P_S, to 71%.

(5) The experimental results for slender CFPT specimens were compared with the predicted results from the two proposed equations; {B-EQ.1-[21]} and {C- Eq.2-Present study}, showing good agreement.

CFPT is a technique with low cost for the increment of ductility of compression elements. The material properties need to be engineered to achieve the desired performance. Future work should cover the effect of flexure and shear to obtain complete interaction diagrams and understand the fundamental behavior.

REFERENCES

Abdalla, K.M., Al-Rousan, R.Z., Alhassan, M.A., and Lagaros, N.D. (2019). "Modeling and analysis of optimized rectangular RC columns confined with CFRP composites." Jordan Journal of Civil Engineering, 13 (2), 325-334.

Abdelkarim, O. I., and El-Gawady, M. A. (2015). "Concrete-filled large deformable FRP tubular columns under axial compressive loading." Fibers, 3, 432-449.

Abdulla, N.A. (2020). "Concrete encased with engineering plastics." Journal of Civil Engineering and Construction, 9 (1), 31-41.

American Concrete Institute. (2008). "Guide for the design and construction of externally bonded FRP systems for strengthening concrete structures." ACI 440.2R-08, Farmington Hills, Mich.

Choi, H. (2019). "Applicability evaluation of short concrete columns using recycled coarse aggregate in an existing column design model." Jordan Journal of Civil Engineering, 13 (1), 70-84.

Fakharifar, M., and Chen, M.G. (2016). "Compressive behavior of FRP-confined concrete filled PVC tubular columns." Composite Structures, 141, 91-109.

Gu, D. S., Wu, Y. F., Wu, G., and Wu, Z. S. (2012). "Plastic hinge analysis of FRP-confined circular concrete columns." Construction and Building Materials, 27 (1), 223-233.

Kurt, E.C. (1978). "Concrete filled structural plastic columns." ASCE Proceedings, 104 ST1, 55-63.

Kwak, H.G., and Kim, J. K. (2004). "Ultimate resisting capacity of slender RC columns." Computers and Structures, 82, 901-915.

Lopes, S.M.R., and Bernardo, L.E.A. (2003)." Plastic rotation capacity of high-strength concrete beams." Materials and Structures, 36, 22-31.

Paulay, T., and Priestley, M.J.N. (1992). "Seismic design of reinforced concrete and masonry buildings." Wiley, New York, 27.

Rahai, A. R., Alinia, M. M., and Salehi, S. M. F. (2009). "Cyclic performance of buckling restrained composite braces composed of selected materials." International Journal of Civil Engineering, 7(1).

Tao, Z., and Yu, Q. (2008). "Behavior of CFRP-strengthened slender square RC columns." Magazine of Concrete Research, 60 (7), 523-533.

Timoshenko, S.P., and Goodier, J. N. (1987)."Theory of elasticity". 3rd Edn., International Student Edition.

Wu, Y. F., and Jiang, C. (2014). "Effect of confinement on plastic hinge length of RC square columns." 23rd Australasian Conference on the Mechanics of Structures and Materials (ACMSM23), Byron Bay, Australia, 9-12.

Yan, H., Liu, F.Q., and Gardner, L. (2015). "Post-fire behavior of slender reinforced concrete columns confined by circular steel tubes." Thin-Walled Structures, 87, 12-29.